High Power Laser Science and Engineering, (2023), Vol. 11, e8, 6 pages.
doi:10.1017/hpl.2023.2

HIGH POWER LASER SCIENCE AND ENGINEERING

RESEARCH ARTICLE

High-performance 800–1050 nm seed pulses based on spectral broadening and filtering for petawatt lasers

Wenhai Liang[1,2], Renjing Chen[1,2], Yilin Xu[1,2], Yaping Xuan[1,2], Peng Wang[1,3], Jun Liu[1,2,3], and Ruxin Li[1,2,3]

[1] *State Key Laboratory of High Field Laser Physics and CAS Center for Excellence in Ultra-intense Laser Science, Shanghai Institute of Optics and Fine Mechanics, Chinese Academy of Sciences, Shanghai, China*

[2] *Center of Materials Science and Optoelectronics Engineering, University of Chinese Academy of Sciences, Beijing, China*

[3] *Zhangjiang Laboratory, Shanghai, China*

(Received 28 August 2022; revised 28 November 2022; accepted 30 December 2022)

Abstract

High-performance 86 μJ, 11.2 fs pulses with a spectrum range of 800–1050 nm are generated based on 1030 nm, 190 fs Yb femtosecond pulses by using multi-plate-based spectral broadening and filtering. Taking advantage of single beam configuration, the obtained pulses have excellent power and spectral stabilities. Since the output spectrum is obtained by spectrally filtering the broadened components, the temporal contrast of the output pulses is enhanced by at least four orders of magnitude. Together with the robust and simple setup, the proposed method is expected to be a competitive option for the generation of seed pulses for 10s–100s petawatt lasers.

Keywords: pulse compression; seed pulse; spectral broadening; temporal contrast

1. Introduction

Petawatt (PW) lasers can introduce extremely high values to many physical parameters, such as the pressure, temperature, electric field and magnetic field. With these controllable extreme physical conditions, researches such as laboratory astrophysics, particle acceleration, nuclear physics, and nonlinear quantum electrodynamics, have become hot topics in recent years[1,2]. As the peak power of an ultra-intense laser increases to tens or hundreds of PW[3], optical parametric chirped pulse amplification (OPCPA) is the only choice because deuterated potassium dihydrogen phosphate (DKDP) is the only crystal large enough to support the corresponding high energy. Moreover, the central wavelength of the seed pulse is confined to about 910 nm[4] in order to achieve broad gain bandwidth with DKDP-based OPCPA. Besides the focused intensity, laser pulses with high temporal contrast are also of vital importance in ultrahigh intensity physics processes to avoid destructive prepulses[5]. To achieve PW pulses with high temporal contrast, the generation of high-temporal-contrast seed pulses is the first step.

Except for one that achieved 560 TW peak power using a Cr:forsterite master oscillator[6], several methods have been proposed so far to generate seed pulses at the central wavelength of 910 nm, which can be divided into two categories based on the laser sources. The first category is based on Ti:sapphire femtosecond laser pulses with a relatively broad spectrum at 800 nm central wavelength[7–9]. In 2018, the combination of a hollow-core fiber (HCF) system and cross-polarization generation was used to generate a 4 μJ broadband seed pulse at 910 nm for few-cycle pulse amplification[7]. Even though only simple collinear geometry configuration is needed, HCF technology is sensitive to alignment with usually a fiber coupling efficiency of about 60%. By combining the techniques of cascaded optical parametric amplification (OPA) and second-harmonic generation, broad-bandwidth carrier-envelope-phase-stabilized seed pulses were obtained[8]. Note that as high as 250 μJ pulses with a high temporal contrast and broadband spectrum were generated from a single-stage four-wave mixing (FWM) process in 2019[9]. The second category is based on Yb femtosecond laser pulses with a relatively narrow spectrum at 1030 nm central wavelength[10,11]. In comparison to the Ti:sapphire laser, the Yb femtosecond laser has better energy stability and long-term operation reliability, which have been widely verified in industry for years. Through white-light generation, difference frequency generation and two stages of OPA processes, a 910 nm seed pulse with pulse

Correspondence to: Jun Liu, State Key Laboratory of High Field Laser Physics and CAS Center for Excellence in Ultra-intense Laser Science, Shanghai Institute of Optics and Fine Mechanics, Chinese Academy of Sciences, Shanghai 201800, China. Email: jliu@siom.ac.cn

energy of 80 μJ was obtained in 2017[10]. More recently, a noncollinear OPA system pumped by a Yb^{3+}-based chirped pulse amplification (CPA) system was presented to generate 11 fs pulses with 230 nm full width at half maximum (FWHM) bandwidth[11]. Apparently, multiple stages of complicated nonlinear processes were used in most of the reported methods to generate broadband seed pulses with a considerable temporal contrast. In three-wave or FWM processes, the requirement of simultaneous spatial and temporal synchronization made the optical setups complicated, and affected the output stability in both energy and spectral profiles.

On the other hand, spectral broadening in gases, filaments and bulk media has been widely studied in the past decades to achieve shorter pulse duration[12]. Several third-order nonlinear processes, such as self-phase modulation (SPM), self-focusing, FWM and cross-phase modulation, are the main effects that contribute to the spectral broadening of the output pulse. Owing to the nonlinear processes, the generated new wavelengths should be clean and have high temporal contrast[9]. Recently, a multi-plate optical setup has been proven to be a more effective method for spectral broadening in comparison to other approaches[13]. Since firstly proposed in 2014[14], many works[15,16] have been executed in both Ti:sapphire and Yb femtosecond lasers with the pulse energy ranging from several microjoules to a few joules. A spectrum ranging from 570 to 1300 nm was generated with two stages of multi-plate by using 170 fs pulses from an ytterbium-doped potassium gadolinium tungstate (Yb:KGW) laser, which realized 3.2 fs pulses after dispersion compensating[17]. Through a 5-mm-thick silica plate, laser pulses of several joules were compressed[18]. In 2021, periodic layered Kerr media theory was proposed to generate quasi-stationary solitons that could improve the performance of supercontinuum generation and pulse compression[13].

In this paper, with a 190 fs Yb femtosecond laser, a simple method combining multi-plate spectral broadening with spectral filtering was proposed to generate 86 μJ, 800–1050 nm high-performance seed pulses. The combination of the third-order nonlinear effect and spectral filtering greatly improved the temporal contrast of the seed pulses by at least four orders of magnitude. Since only one input beam was involved, there were no requirements of spatial or temporal synchronization, and the generated seed pulses had no angular dispersion. As a result, the output laser pulses had high energy stability and spectral stability. The pulse duration was shortened from 190 to 11.2 fs, corresponding to a compression ratio of about 18. Based on these excellent characteristics, the generated pulses are excellent seed pulses for 10s–100s PW laser systems[3] and high-repetition OPCPA systems for attosecond science[19].

2. Experimental setup

To achieve a high-performance seed pulse at the central wavelength of 910 nm, the multi-plate-based spectral broadening method was applied in this paper. The experimental setup is shown in Figure 1. A 1-kHz, 1030 nm, 190 fs, 0.92 mJ Yb:KGW laser was used as the light source.

In the first stage (stage 1), the collimated laser beam with a diameter of 4.1 mm was focused to a $1/e^2$ waist of 0.75 mm by a plano-convex lens with a focal length of 2000 mm, which yielded approximately a focal intensity of 1.1 TW/cm^2 at the surface of the first 0.5-mm-thick sapphire (Al_2O_3) plate. Four same sapphire plates were placed in a particular sequence, where the distances between each other were 22.1, 22.1 and 54.7 mm, respectively. The induced B-integral at the first plate was about 1. The output laser beam was collimated by L2 ($f = 1500$ mm), and then compressed by a pair of chirped mirrors (CM1s, UltraFast Innovations, CM39). Afterwards, the laser beam was focused by L3 ($f = 1000$ mm) onto two 2-mm-thick sapphire plates spaced by 47.4 mm. In the second stage (stage 2), the output laser from stage 1 was filtered by a short-pass filter (SP-filter), focused by an $f = 300$ mm lens, and interacted with two 3-mm-thick sapphire plates with a spacing of 11.6 mm. After being collimated by L5 ($f = 1000$ mm), the beam with a diameter of 1.3 mm passed through another chirped mirror pair

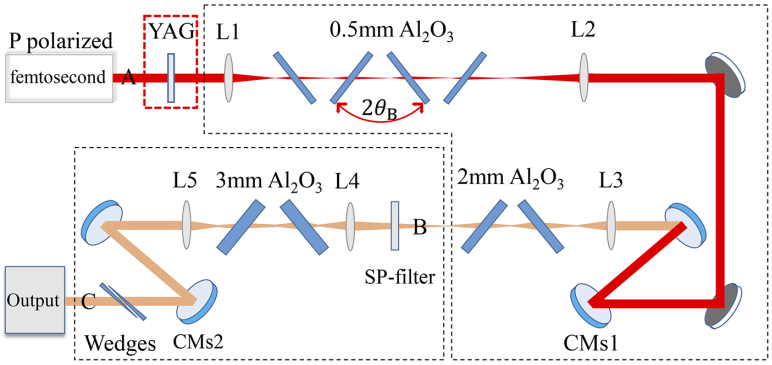

Figure 1. The optical setup. L1–L5 denote anti-reflection coated plano-convex lenses. CMs1 and CMs2 are two pairs of chirped mirrors. SP-filter denotes a dielectric short-pass filter with a cut-off wavelength of 1025 nm. The yttrium aluminum garnet plate is not used in any of the experiments except for the process of contrast measurement using a second-order correlator.

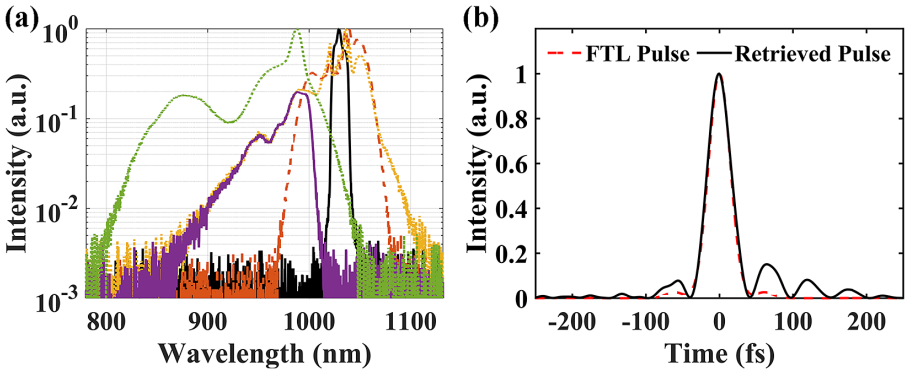

Figure 2. (a) Spectra of the input (black solid curve), after four 0.5-mm-thick sapphire plates (red dashed curve), after two 2-mm-thick sapphire plates (yellow dotted curve), after the SP-filter (purple solid curve) and after the seed pulse (green dotted curve). (b) Retrieved temporal profile after CMs1 and the corresponding FTL pulse.

(CMs2, Thorlabs, DCMP175) and a pair of fused silica wedges for dispersion compensation. In the two stages, inspired by previous researches[13,20], the positions and thicknesses of all plates ensured such moderate spectral broadening that avoided conical emission, filaments and polycyclic phenomena, which were most manifested in strong periodic modulations of the spectrum or the beam profile. In addition, all plates were placed at the Brewster angle to reduce the reflection loss.

3. Results and discussion

The spectra of the input and output pulses after every multi-plate were captured by using a spectrometer (USB4000, Ocean Optics). All the spectral profiles with a logarithmic coordinate in the intensity are shown in Figure 2(a). Except for the filtered-out spectrum after the dielectric SP-filter, all the spectral intensities of the output pulses were normalized. Obviously, the spectrum extended from 1010–1050 to 980–1080 nm at a –23 dB intensity level after the first four 0.5-mm-thick sapphire plates. After four bounces of reflections on CMs1 and a total group delay dispersion (GDD) of –2000 fs^2, an output of a 36 fs compressed pulse was achieved, as shown in Figure 2(b). The temporal profile was characterized by using our home-made all-reflective transient-grating-based self-referenced spectral interference (TG-SRSI) apparatus[21], which was close to the Fourier-transform-limited (FTL) pulse of 33 fs FWHM based on the measured spectrum.

After another two 2-mm-thick sapphire plates, the output pulse spectrum was further broadened from the 980–1080 to the 850–1130 nm spectral range at a –23 dB intensity level, as shown in Figure 2(a). Afterwards, the output pulses were filtered by the SP-filter, as shown in Figure 2(a). By slightly tilting the SP-filter, the 850–1010 nm filtered spectrum had no spectral overlap with that of the input pulse, which ensured an extremely clean pulse with high temporal contrast. After spectral broadening in the following two 3-mm-thick sapphire plates and a B-integral of 5.67 in the former plate, the seed pulse spectrum extended from 800 to 1050 nm at a –23 dB intensity level, as shown in Figure 2(a) with the green dotted curve.

To verify the spectral homogeneity in the spatial domain, the spectra at five different positions on the output laser beam were measured, which showed almost the same spectral range and spectral profile, as shown in Figure 3(a). The result indicated that no spatial chirp was observed on the output laser beam. After dispersion compensating by two bounces of reflections on CMs2 with a total GDD of –350 fs^2 and a pair of fused silica wedges, the output pulse had a compressed pulse duration of 11.2 fs, which was measured by the home-made all-reflective TG-SRSI[21]. As shown in Figure 3(b), the spectrum of the TG reference pulse was broader and smoother than that of the seed pulse. The measured spectrum matched the retrieved spectrum very well, as shown in Figure 3(c). The retrieved temporal profile is shown in Figure 3(d), which is close to the FTL temporal profile with a 10.1 fs FWHM duration.

The power and spectral stabilities at the three positions shown in Figure 1 with A–C were recorded. Since only one input beam was involved in the experimental setup, neither spatial nor temporal synchronization was needed, ensuring the output signal had high stability. The measurement of the spectral stability at each position was carried out with a spectrometer (USB4000, Ocean Optics) connected by an integral sphere with a fiber and a time interval of 1 s. The integral time of the spectrometer was set at 100 ms. As shown in Figures 4(a)–4(c), in 30 minutes, all the spectra exhibit a favorable smoothness and continuity pattern, which indicates excellent spectral stability. By integrating the spectral intensity profiles at every time point, the corresponding power stabilities were obtained, as shown with red curves in Figures 4(d)–4(f). Furthermore, in consideration of the relatively low repetition rate, the PW laser generally works over a long period of time. Therefore, the power stabilities for

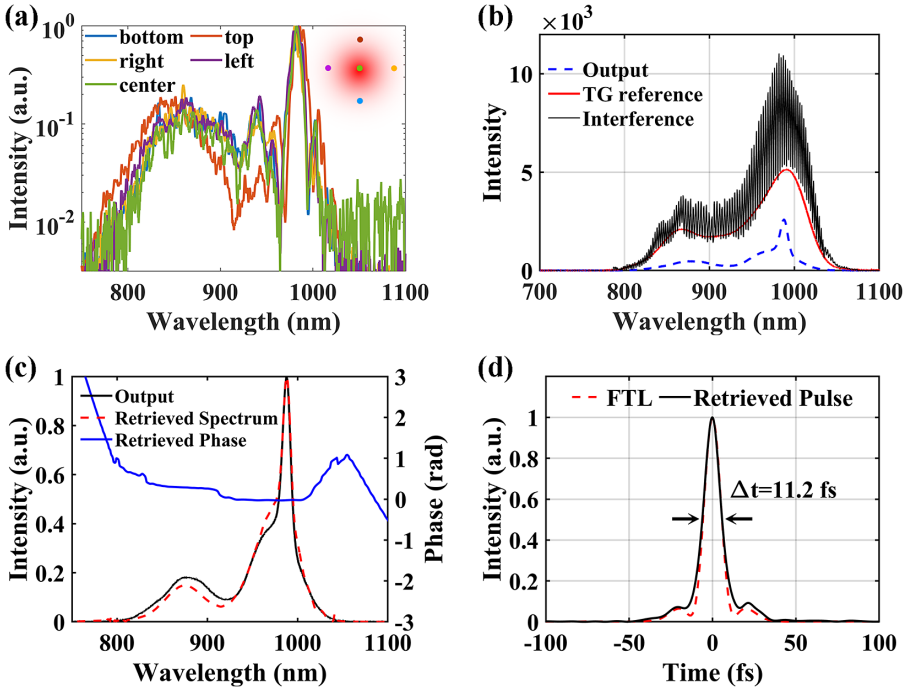

Figure 3. (a) Seed pulse spectra at five different positions. Inset: illustration of the five positions being sampled. (b), (c) TG-SRSI spectra and the retrieved spectral phase. (d) FTL and retrieved TG-SRSI temporal profiles, respectively.

up to 5 hours were also measured and are shown with black curves in Figures 4(d)–4(f), where the root mean squares (RMSs) at points B and C are 0.108% and 0.127% higher, respectively, than that at point A, which was mainly due to the influence of the airflow in the laboratory. In addition, during the measurement of up to 5 hours, the setup has been working properly without aging of the plates and filter.

Taking advantage of high energy efficiency, the 0.92 mJ input pulse energy after CMs1 left was 0.80 mJ, corresponding to an energy loss of 13%. After the SP-filter, the pulse energy decreased to 97 μJ, resulting in a pulse energy of 86 μJ at position C, with an energy transfer efficiency of 89% for stage 2. The total conversion efficiency from the input to the output pulse was about 9.3%, which was still higher than previous single-stage FWM process[9].

The spatial profiles of the input and output laser beams were captured by using a charge-coupled device (BC106, Thorlabs). Figures 5(a)–5(d) show the captured near-field beam profiles of the input beam, after passing one or four plates in stage 1, and the output beam. As no conical emission or multiple rings appeared throughout the whole process, the spatial profiles of all the beams showed excellent Gaussian shapes. The central part with high intensity was smoothed and became smaller, which may be due to the self-focusing effect. The excellent spatial output beams were attributed to the reasonable placements and thicknesses of the plates. A spectrum broader than 980–1080 nm may be achieved by simply placing more plates after the first four Al_2O_3 plates; however, less energy will be transferred to 800–1050 nm in this case.

Unlike the cross-polarization generation process in which the temporal-contrast enhancement is limited by the extinction ratio of the polarizer, the combination of multi-plate spectral broadening and spectral filtering can be used to enhance the temporal contrast without a polarizer. Since the SPM effect is dependent on the peak power, only the main pulse experienced a significant spectral broadening, while the low-intensity part of the pulse remained unaffected. The temporal contrast was enhanced by suppressing the low-intensity parts of the pulse with a spectral filter that blocked the wavelengths of the initial input pulse[22]. To verify the pulse cleaning ability, second-order autocorrelation (SAC) was chosen[23] instead of other methods[24] because of the relative low pulse energy and that it is sufficient to illustrate the pulse cleaning capability of the setup.

The optical setup of SAC for temporal-contrast measurement was almost the same as in Ref. [23]. In brief, a 1-mm-thick yttrium aluminum garnet (YAG) crystal was located directly after the Yb laser to intentionally induce a reduced post pulse, as shown in Figure 1. For the YAG crystal, the reflectivity at 0-degree incidence is about 8.4%. In the SAC setup, one 2-mm-thick 50/50 beam splitter was used to split the laser beam. A 0.5-mm-thick β-barium-borate crystal was used to generate the sum-frequency signal, which was then detected by a USB4000 spectrometer with 100 ms integration time. The intensity of the sum-frequency signal at every delay time was obtained by integrating the measured spectral intensity over the spectral range of 400–550 nm. In case the sum-frequency signal from –4500 to 4500 fs was too strong to be detected by the spectrometer, the range

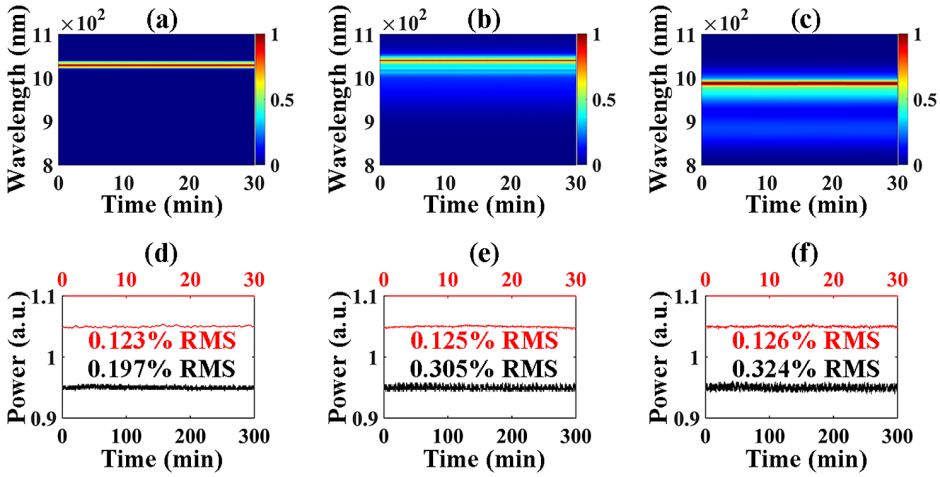

Figure 4. (a)–(c) Spectral stabilities characterized at positions of A–C. (d)–(f) The corresponding power stabilities by integrating spectral intensity (red curve) and measured by a power meter (black curve).

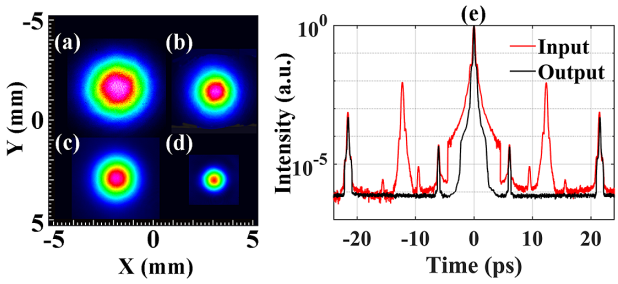

Figure 5. (a)–(d) Near-field beam profiles of the input, after passing one plate in stage 1 and four plates in stage 1, and the output. (e) SAC intensities of the input and output pulses.

of scanning time was segmented to ensure that all signals in the picture were properly represented. For the input, the attenuation factor was about 200 from –4500 to –450 fs and 450 to 4500 fs. From –450 to 450 fs, the attenuation factor was about 2000. For the output, the attenuation factor was about 200 from –4500 to –70 fs and 70 to 4500 fs. From –70 to 70 fs, the attenuation factor was about 2000. All the attenuation factors and the moment of adding the attenuator were chosen with the aim of obtaining a complete and unsaturated SAC curve, which benefited from the techniques associated with third-order correlators. For the input of Figure 5(e), the jump at –4500 fs was because the attenuation factor was still a little larger, as was the jump at 4500 fs. The real contrast did not have the jumps. Figure 5(e) shows the SAC intensities of both the input and the output pulses when the delay time varied from –24 to 24 ps with 10 fs/step. It is clear that the temporal contrast of the output seed pulse is greatly improved compared with that of the input pulse. The post pulse introduced by the inserted YAG plate had a delay time of 12.26 ps with a relative intensity of about 10^{-2}, which was consistent with the calculation based on the Fresnel reflection. There was no peak at the same delay time for the output pulse, where the background noise had a relative intensity of about 10^{-6}, limited by the SAC method. At least four orders of magnitude improvement on the temporal contrast was verified. The real temporal-contrast improvement of the output seed pulse should be much higher than the measurement result, which was limited by the low energy, the noise of the scattering medium and the sensitivity of the spectrometer. The two peaks at ±6.02 and ±21.65 ps were due to the front-to-back reflections by the 0.5-mm-thick beta barium borate (BBO) crystal and the beam splitter used in the SAC, respectively. In addition, the peaks at ±9.46 and ±15.59 ps for the input only were also cleaned by the spectral broadening and spectral filtering process.

4. Conclusions

In summary, based on narrow bandwidth Yb femtosecond pulses at 1030 nm, we have demonstrated the generation of pulses in the 800–1050 nm spectral range with compressed pulse duration and improved temporal contrast by using a multi-plate-based spectral broadening and spectral filtering setup. The third-order nonlinear effects in multi-thin plates, including SPM and self-focusing, contribute to spectral broadening and temporal-contrast enhancement. In our proof-of-principle experiment, the pulse duration was compressed from 190 to 11.2 fs, resulting in a compression ratio of about 18. The temporal contrast was improved by at least four orders of magnitude. Furthermore, the output pulses had excellent power stability and spectral stability. By using spherical reflective mirrors instead of lenses, less group velocity and phase velocity will be induced to the seed pulses with bandwidths of about 200 nm[25]. In the future, higher energy and a broader spectral range are expected to be obtained by increasing the input pulse energy or adding another stage. The proposed method is also promising for

generating few-cycle pulses, which can be used in pump-probe experiments.

Acknowledgements

The authors would like to thank Prof. Quanzhong Zhao for offering the Yb femtosecond laser system. This work was supported by the Shanghai Municipal Natural Science Foundation (No. 20ZR1464500), the National Natural Science Foundation of China (NSFC) (Nos. 61905257 and U1930115) and the Shanghai Municipal Science and Technology Major Project (No. 2017SHZDZX02).

References

1. H. Daido, M. Nishiuchi, and A. S. Pirozhkov, Rep. Prog. Phys. **75**, 056401 (2012).
2. D. E. Cardenas, T. M. Ostermayr, L. Di Lucchio, L. Hofmann, M. F. Kling, P. Gibbon, J. Schreiber, and L. Veisz, Sci. Rep. **9**, 7321 (2019).
3. C. N. Danson, C. Haefner, J. Bromage, T. Butcher, J.-C. F. Chanteloup, E. A. Chowdhury, A. Galvanauskas, L. A. Gizzi, J. Hein, D. I. Hillier, N. W. Hopps, Y. Kato, E. A. Khazanov, R. Kodama, G. Korn, R. Li, Y. Li, J. Limpert, J. Ma, C. H. Nam, D. Neely, D. Papadopoulos, R. R. Penman, L. Qian, J. J. Rocca, A. A. Shaykin, C. W. Siders, C. Spindloe, S. Szatmári, R. M. G. M. Trines, J. Zhu, P. Zhu, and J. D. Zuegel, High Power Laser Sci. Eng. **7**, e54 (2019).
4. A. Lyachev, I. O. Musgrave, Y. Tang, C. Hernandez-Gomez, I. N. Ross, M. Galimberti, O. V. Chekhlov, and J. Collier, Opt. Express **19**, 15824 (2011).
5. P. Antici, J. Fuchs, E. d'Humières, E. Lefebvre, M. Borghesi, E. Brambrink, C. A. Cecchetti, S. Gaillard, L. Romagnani, Y. Sentoku, T. Toncian, O. Willi, P. Audebert, and H. Pépin, Phys. Plasmas **14**, 030701 (2007).
6. V. V. Lozhkarev, G. I. Freidman, V. N. Ginzburg, E. V. Katin, E. A. Khazanov, A. V. Kirsanov, G. A. Luchinin, A. N. Mal'shakov, M. A. Martyanov, O. V. Palashov, A. K. Poteomkin, A. M. Sergeev, A. A. Shaykin, and I. V. Yakovlev, Laser Phys. Lett. **4**, 421 (2007).
7. A. Kessel, V. E. Leshchenko, O. Jahn, M. Krüger, A. Münzer, A. Schwarz, V. Pervak, M. Trubetskov, S. A. Trushin, F. Krausz, Z. Major, and S. Karsch, Optica **5**, 434 (2018).
8. B. Shao, Y. Li, Y. Peng, P. Wang, J. Qian, Y. Leng, and R. Li, Opt. Lett. **45**, 2215 (2020).
9. P. Wang, X. Shen, Z. Zeng, J. Liu, R. Li, and Z. Xu, Opt. Lett. **44**, 3952 (2019).
10. R. Budriūnas, T. Stanislauskas, J. Adamonis, A. Aleknavičius, G. Veitas, D. Gadonas, S. Balickas, A. Michailovas, and A. Varanavičius, Opt. Express **25**, 5797 (2017).
11. I. Tamer, M. Hellwing, Y. Azamoum, M. Hornung, S. Keppler, F. Schorcht, J. Hein, and M. C. Kaluza, Opt. Express **28**, 19034 (2020).
12. T. Nagy, P. Simon, and L. Veisz, Adv. Phys. X **6**, 1845795 (2021).
13. S. Zhang, Z. Fu, B. Zhu, G. Fan, Y. Chen, S. Wang, Y. Liu, A. Baltuska, C. Jin, C. Tian, and Z. Tao, Light Sci. Appl. **10**, 53 (2021).
14. C.-H. Lu, Y.-J. Tsou, H.-Y. Chen, B.-H. Chen, Y.-C. Cheng, S.-D. Yang, M.-C. Chen, C.-C. Hsu, and A. H. Kung, Optica **1**, 400 (2014).
15. J. E. Beetar, S. Gholam-Mirzaei, and M. Chini, Appl. Phys. Lett. **112**, 051102 (2018).
16. M. Stanfield, N. F. Beier, S. Hakimi, H. Allison, D. Farinella, A. E. Hussein, T. Tajima, and F. Dollar, Opt. Express **29**, 9123 (2021).
17. C.-H. Lu, W.-H. Wu, S.-H. Kuo, J.-Y. Guo, M.-C. Chen, S.-D. Yang, and A. H. Kung, Opt. Express **27**, 15638 (2019).
18. V. Ginzburg, I. Yakovlev, A. Kochetkov, A. Kuzmin, S. Mironov, I. Shaikin, A. Shaykin, and E. Khazanov, Opt. Express **29**, 28297 (2021).
19. P. Rudawski, A. Harth, C. Guo, E. Lorek, M. Miranda, C. M. Heyl, E. W. Larsen, J. Ahrens, O. Prochnow, T. Binhammer, U. Morgner, J. Mauritsson, A. L'Huillier, and C. L. Arnold, Eur. Phys. J. **69**, 70 (2015).
20. B. Shao, Y. Li, Y. Peng, W. Li, J. Qian, Y. Leng, and R. Li, IEEE Photonics J. **13**, 3300108 (2021).
21. Z. Si, X. Shen, J. Zhu, L. Lin, L. Bai, and J. Liu, Chin. Opt. Lett. **18**, 021202 (2020).
22. J. Buldt, M. Müller, R. Klas, T. Eidam, J. Limpert, and A. Tünnermann, Opt. Lett. **42**, 3761 (2017).
23. J. Liu, K. Okamura, Y. Kida, and T. Kobayashi, Opt. Express **18**, 22245 (2010).
24. P. Wang, X. Shen, J. Liu, and R. Li, Adv. Photonics **1**, 056001 (2019).
25. Z. Bor, Opt. Lett. **14**, 119 (1989).